Crystallization and Aggregation Behaviors of Calcium Carbonate in the Presence of Poly(vinylpyrrolidone) and Sodium Dodecyl Sulfate

Qiang Shen,*,†,‡ Hao Wei,‡ Liancheng Wang,† Yong Zhou,‡ Ying Zhao,‡ Zhiqing Zhang,† Dujin Wang,*,‡ Guiying Xu,† and Duanfu Xu‡

Key Laboratory for Colloid and Interface Chemistry of Education Ministry, School of Chemistry & Chemical Engineering, Shandong University, Ji'nan 250100, China, and State Key Laboratory of Polymer Physics & Chemistry, Institute of Chemistry, Chinese Academy of Sciences, Beijing 100080, China

Received: April 22, 2005; In Final Form: July 12, 2005

An anionic surfactant interacts strongly with a polymer molecule to form a self-assembled structure, due to the attractive force of the hydrophobic association and electrostatic repulsion. In this crystallization medium, the surfactant-stabilized inorganic particles adsorbed on the polymer chains, as well as the bridging effect of polymer molecules, controlled the aggregation behavior of colloidal particles.[1] In this presentation, the spontaneous precipitation of calcium carbonate ($CaCO_3$) was conducted from the aqueous systems containing a water-soluble polymer (poly(vinylpyrrolidone), PVP) and an anionic surfactant (sodium dodecyl sulfate, SDS). When the SDS concentrations were lower than the onset of interaction between PVP and SDS, the precipitated $CaCO_3$ crystals were typically hexahedron-shaped calcite; the increasing SDS concentration caused the morphologies of $CaCO_3$ aggregates to change from the flower-shaped calcite to hollow spherical calcite, then to solid spherical vaterite. These results indicate that the self-organized configurations of the polymer/surfactant supramolecules dominate the morphologies of $CaCO_3$ aggregates, implying that this simple and versatile method expands the morphological investigation of the mineralization process.

1. Introduction

Biological materials have unique structures and morphologies, which acquire much better performance than the relatively crude minerals. More than 60 kinds of inorganic minerals have been found in various organisms. For example, the proteins/$CaCO_3$ hybrids in mollusc shells have superior mechanical properties, which arouse great scientist interest in understanding the natural biomineralization process.[2−4] Calcium carbonate is one of the most common biological minerals, which has polymorphs of calcite, aragonite, and to a lesser extent of amorphous state, vaterite and monohydrate in calcareous structures of organisms.[5] In different calcareous structures, the size, habit, and aggregation state of these polymorphic species are different, resulting in different characteristics and performance. The template-controlled mineralization in natural systems is due to many basic underlying mechanisms such as molecular recognition, local supersaturation, complexation, and the formation of molecular superstructures for size and shape control.

In these fast-reactive crystallization processes, the calcium ions and carbonate groups combine into the amorphous $CaCO_3$, the most instable solid-state phase. Then, the initially formed $CaCO_3$ is transformed within a few minutes to a mixture of severe crystalline $CaCO_3$. The transformed carbonates are vaterite and calcite at low temperatures (14−30 °C) and aragonite and calcite at high temperatures (60−80 °C). At intermediate temperatures (40−50 °C) the transformed phase contains all of the three variations.[6] The stability of these $CaCO_3$ crystalline polymorphs decreases in the following order: vaterite < aragonite < calcite. Actually, the stability and lifetime of these polymorphic species mainly depend on the properties of additives and their own solubilities in aqueous solution.[6−8] Recently, various self-assemblies of organic compounds were used as templates to synthesize $CaCO_3$ crystals and to control their morphologies, polymorphs, and metastable phases.[9−20] Although the influence of uncharged polymers,[21,22] anionic surfactants, or the polymer−surfactant mixtures[23−29] on the crystallization processes of inorganic crystals have been investigated, nevertheless, the aqueous systems containing polymer−surfactant mixture have not been used for the crystallization and aggregation behavior of calcium carbonate. We decided to use PVP−SDS solutions as crystallization media for $CaCO_3$ on the basis of the following considerations:

(a) SDS polar groups act as active sites for $CaCO_3$ nucleation,[1] due to their electrostatic interaction with calcium ions. When the surfactants simultaneously associate with polymer chains through hydrophobic effectiveness, the aggregation states of polymer/surfactant supramolecules could control the size, shape, morphology, and polydispersity of $CaCO_3$ crystals.

(b) The PVP dispersion capability for the solid particles, as well as the mechanical stirring, prevents the direct precipitation of $CaCO_3$. This favors the nucleation, growth, transformation from vaterite to calcite, or aggregation of $CaCO_3$ crystalline particles on the surfaces of PVP/SDS aggregates.

Biomimetic mineralization is interesting not only for the understanding of the formation of natural materials, but also for the formation of new hybrid materials from commonly available cheap educts. Some of the above points have previously been verified.[1,22] However, the structural relationship between the PVP/SDS supramolecules[30−36] and the inorganic minerals is too ambiguous to be widely used for the biomimetic

* Address correspondence to these authors. E-mail: qshen@sdu.edu.cn (Dr. Q. Shen) and djwang@iccas.ac.cn (Prof. D. J. Wang).

† Key Laboratory for Colloid and Interface Chemistry of Education Ministry.

‡ State Key Laboratory of Polymer Physics & Chemistry.

10.1021/jp052094a CCC: $30.25
Published on Web 09/09/2005

syntheses of functionally composite materials. This involves the crystallization and aggregation processes of inorganic minerals, which is the subject of the present paper.

2. Experimental Section

2.1. Chemicals and solution preparation: All chemicals, $CaCl_2$, Na_2CO_3, SDS, and PVP (molecular weight $\approx$ 30 000), are of A. R. grade and were used without further purification. Doubly deionized water was used to prepare aqueous $CaCl_2$ and Na_2CO_3 solutions just before each experiment. For these reactive crystallization systems, the PVP was previously added into both of the aqueous $CaCl_2$ and Na_2CO_3 solutions, respectively, while the SDS was only added into Na_2CO_3 solution before mixing.

2.2. Structural characterization of PVP/SDS complex: At 26 ± 0.2 °C, surface tension (γ) measurements were conducted by Krüss-K12 processor tensiometer according to the Wilhelmy gravimetric method. Normally, in the curve between γ and the logarithm of surfactant concentration, the transition point represents the critical concentration for the onset of aggregates.[30−36]

2.3. $CaCO_3$ precipitation experiments: $CaCO_3$ crystals were precipitated by means of rapidly pouring 0.1 M $CaCl_2$ solution (100 mL) into a 300 mL beaker containing an equal volume of 0.1 M Na_2CO_3 solution. The crystallization system was continuously stirred at a constant rate of 200 rpm by the Teflon-coated magnetic stirring bar, unless it was emphasized in the context. The resulting $CaCO_3$ particles were kept in their incubation systems for 10 h to allow further crystal growth by Ostwald ripening and to see the template effects of organic aggregates. During the precipitation and incubation process, the reactive systems were kept at 26 ± 0.2 °C in a thermostatic bath and at a constant pH value ($\approx$7.0). Filtered through cellulose nitrated/acetate membrane filters (0.2 μm) and rinsed three times with doubly deionized water, the $CaCO_3$ crystals were dried in a vacuous desiccator cabinet at room temperature for at least 24 h and used for measurements. The advantage of this method is to eliminate all other affecting factors than the supramolecular structure of additives.

2.4. Crystal characterization: All samples were Au coated prior to examination by a Hitachi S-4300 scanning electron microscope (SEM), fitted with a field emission source and operating at an accelerating voltage of 15 kV. The particle size and size distribution for the obtained $CaCO_3$ crystals were calculated by using an image analysis program (Scion Image-PC version).

Transmission electron microscopy (TEM) images were recorded by a Hitachi H-800 transmission electron microscope operating at 200 kV. The samples dispersed in water were directly deposited on a carbon film supported by a copper grid.

The X-ray diffraction (XRD) patterns were collected on a Rigaku D/max-2400 powder X-ray diffractometer with Cu Kα radiation (40 kV, 120 mA). The 0.02° steps per 25 s and the 2θ range from 20 to 60° were selected to analyze the crystal structure and orientation.

Micro-IR spectrum measurements were performed on a Nicolet Magna-750 IR spectrometer, with scanning times of 100, and resolution of 4 cm^{-1}.

3. Results and Discussion

3.1. Formation of the possible PVP/SDS supramolecules in crystallization media: The plot of the surface tension (γ) of aqueous surfactant system against the logarithm of surfactant concentration shows one break point at critical micellization concentration (CMC), due to hydrophobic association (attractive force) and electrostatic interaction (repulsive force). Addition of inorganic salt screens electrostatic headgroup repulsion between molecules of ionic surfactant, resulting in a low CMC value. For example, the addition of 0.1 M sodium chloride causes the CMC value of SDS to change from 9.0×10^{-3} to 1.6×10^{-3} M.[31,32] Further addition of PVP into the SDS/NaCl (0.1 M) systems caused the plot of γ against log[SDS] to reveal two transition points (T_1 and T_2) shown in Figure 1.

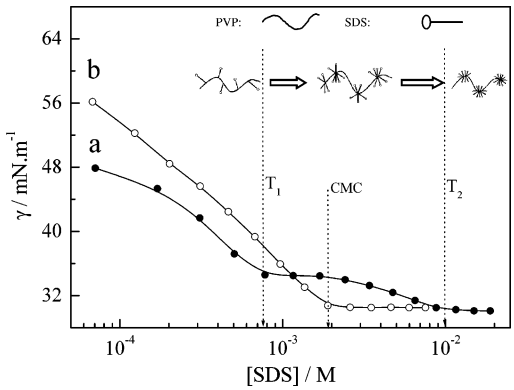

Figure 1. Variation of the surface tension with SDS concentration in the presence of 1.0 g/L PVP + 0.1 M NaCl (a, solid symbol) or 0.1 M NaCl (b, open symbol) at 26 °C. T_1 represents the onset of the interaction between PVP and SDS, T_2 the saturation point of beads formed by SDS on PVP backbone, CMC the critical micellization concentration of SDS in the presence of 0.1 M NaCl. Inserts show the structural evolvement of the PVP/SDS supramolecule with the increase of SDS concentration.

The first break point, T_1, indicates the onset of the formation of the PVP/SDS supramolecule occurring at a SDS concentration of 7.5×10^{-4} M (critical aggregation concentration, CAC), while the second transition point of T_2 at 1.0×10^{-2} M indicates that PVP molecules are saturated with SDS molecules to form complete PVP/SDS supramolecules.[37] Initially, a single SDS molecule starts to be bound to a hydrophobic site of PVP molecules (the left insert in Figure 1) at the low SDS concentration of T_1, then several SDS molecules are bound to each hydrophobic site (the middle insert in Figure 1) until the formation of SDS "beads" in PVP chains at the T_2 point (the right insert in Figure 1). Under a definite condition SDS molecules aggregate into micelles, retaining the size polydispersity with almost the same aggregation number.[38] It is due to the bead−bead electrostatic repulsion that each polymer chain only accommodates a limited number of beads. After the T_2 point the aggregation phenomenon finishes, and surfactant molecules will go into the solution again until normal SDS micelles are formed. This indicates that superstructural conformations between the anionic surfactant and the uncharged polymer exist in the bulk phase where crystallization takes place.

3.2. Influence of SDS concentration on $CaCO_3$: After the rapid mixing of equal volumes of 0.1 M $CaCl_2$ + 1.0 g/L PVP and 0.1 M Na_2CO_3 + 1.0 g/L PVP + SDS (at different concentration) solutions, the spontaneous precipitation of $CaCO_3$ particles occurred, resulting in the crystallization media of 1.0 g/L PVP + 0.1 M NaCl + SDS as described in the first paragraph. Although the influence of the resulting NaCl on $CaCO_3$ crystallization has never been discussed,[9−20] it should affect the structure of PVP/SDS supramolecules. The SEM images of $CaCO_3$ crystals sampled at various SDS concentrations are shown in Figure 2. All of the crystal aggregates have sizes in the micrometer range (from 1.6 to 8.6 μm), showing different morphology and polydispersity with varied SDS concentration.

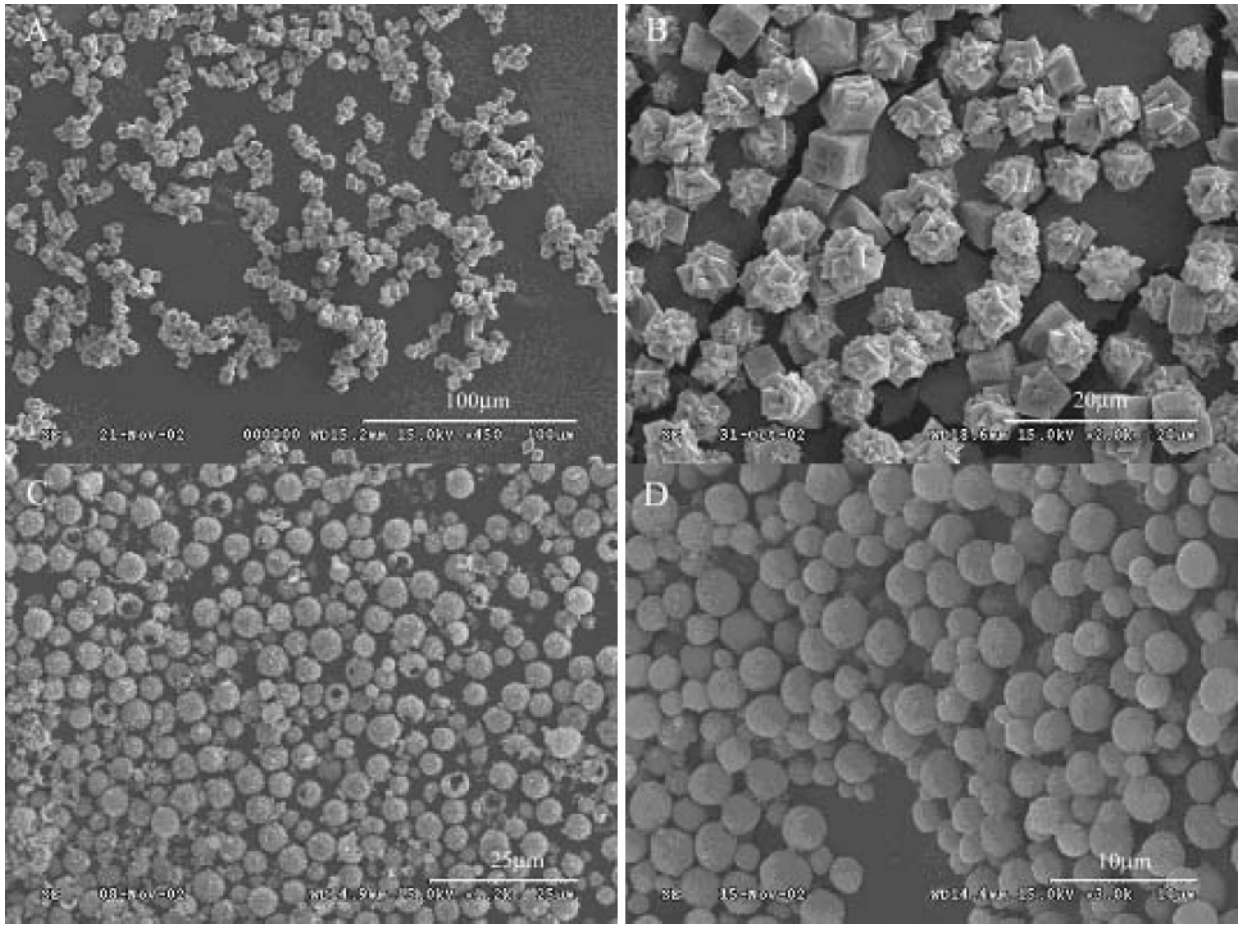

Figure 2. SEM images of the $CaCO_3$ crystals precipitated from the mixing systems of PVP (1.0 g/L) and SDS: A, B, C, and D represent SDS concentrations at 2.5×10^{-4}, 1.0×10^{-3}, 5.0×10^{-3}, and 5.0×10^{-2} M, respectively.

From curve a in Figure 1, SDS concentration was divided into four regions by three dashed lines at T_1, CMC, and T_2. When the SDS concentration was lower than that of T_1 (CAC), surfactant molecules were adsorbed at the air/water interface. Although the SDS headgroups preferred to interact with calcium ions in the crystallization systems,[1,39] the dilute SDS concentration have almost no influence on the generation of $CaCO_3$ crystals, resulting in $CaCO_3$ particles with an average size of 5.6 ± 0.7 μm (Figure 2A). If the headgroups of SDS molecules served as nucleation sites,[24−25,40] the bridging effect of PVP molecules should cause several grown rhombohedral $CaCO_3$ particles to aggregate linearly in Figure 2A.

When SDS concentration was in the region of T_1 and CMC, several SDS molecules clustered at one hydrophobic site in PVP backbones. The growth mechanism controlled by nucleation causes several $CaCO_3$ crystals to aggregate into flower-shaped superstructures 6.3 ± 0.8 μm in size (Figure 2B). In the region of CMC and T_2, the beads in PVP/SDS supramolecular chains serve as spherical templates to generate hollow spheres of $CaCO_3$ crystals in the precipitation system (Figure 2C). It seems that, before T_2, both the nucleation and growth mechanism control the morphologies of $CaCO_3$ aggregates. Scion Image analyses show that the sizes of these hollow spherical aggregates (Figure 2C) range from 3.2 to 8.6 μm. It is normal that the size of grown particles decreases with increasing the concentration of organic additives.[22] Here, Most of these hollow spheres with an average size of 5.9 ± 1.0 μm, as well as most of the flower-shaped aggregates shown in Figure 2B, have a bigger mean size than that of rhombohedrons shown in Figure 2A, suggesting the existence of organic templates.

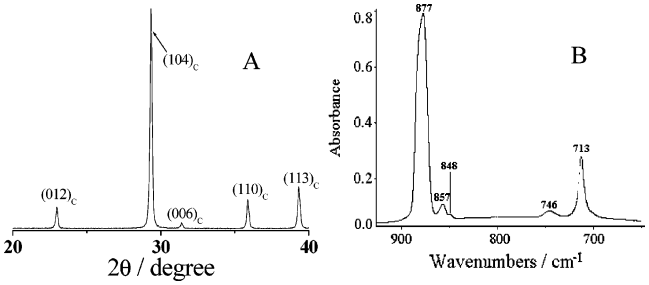

Figure 3. XRD (A) and FT-IR (B) spectral characteristics of the $CaCO_3$ crystals precipitated from the mixing systems of PVP (1.0 g/L) and SDS.

When the SDS concentration was higher than that of T_2, the resulting $CaCO_3$ particles also showed the spherical morphology (Figure 2D). These spheres were proved not to be the core−shell structure by TEM observations. The average particle size was calculated to be 2.9 ± 0.4 μm in diameter, much smaller than those listed before, which indicates that the active sites for $CaCO_3$ nucleation are so numerous that the nucleation effectiveness dominates in the system of 1.0 g/L PVP + 5.0×10^{-2} M SDS.[24−25,40]

3.3. XRD characterization: All of the inorganic samples listed above show the same XRD spectrum signature of the synthetic calcite except for these spherical particles shown in Figure 2D. The XRD pattern (Figure 3A) shows the characteristic reflection at *d* spacings of 3.87, 3.04, 2.84, 2.50, and 2.29 Å corresponding to *hkl* of 012, 104, 006, 110, and 113, respectively. The FT-IR absorption bands (Figure 3B) at 877, 848, and 713 cm^{-1} are assigned to calcite, while the absorption

TABLE 1: XRD Data of the Crystallographic Orientation of Calcite Crystals Precipitated from Different Systems Containing PVP (1.0 g/L), SDS (5.0×10^{-3} M), and the PVP (1.0 g/L)/SDS (5.0×10^{-3} M) Supramolecules

	standard	PVP		SDS		PVP/SDS	
hkl	intensity,[a] *I**	*I*[b]	% *hkl* [c]	*I*[b]	% *hkl* [c]	*I*[b]	% *hkl* [c]
012	12	1032	5.99	2721	8.65	2854	8.46
104	100	15173	10.56	26963	10.29	29714	10.57
110	14	1711	8.51	3558	9.70	3885	9.87
113	18	2451	9.48	5294	11.22	5757	11.38
202	18	2032	7.86	4418	9.37	4645	9.18
024	5	935	13.01	1631	12.45	1695	12.06
018	17	3154	12.92	4280	9.61	4885	10.22
116	17	3180	13.02	4918	11.04	5353	11.20
211	4	455	7.92	835	7.97	869	7.73
122	8	1232	10.72	2035	9.71	2099	9.33

[a] JCPDS 5-0586 data [% *I*] showing the intensities of peaks in the XRD profile for randomly oriented calcite powder. [b] The intensities of peaks in XRD spectra of synthetic calcite crystals precipitated from different solutions. [c] Percentage of calcite crystals in different orientations calculated by means of eq 1.

band at 746 cm^{-1} indicates the coexistence of vaterite.[41−43] The thermodynamically unstable polymorph (i.e., vaterite) stabilized by the mixture of 1.0 g/L PVP + 5.0×10^{-2} M SDS suggests that, at this SDS concentration, the transformation of vaterite to the thermodynamically stable calcite is partly prohibited. [6−8]

The intensities of peaks in the standard XRD spectra of randomly oriented calcite powders (I^*_{hkl}) were normalized to quantitatively analyze the orientational uniformity of calcite synthesized from different precipitation systems (I_{hkl}).[44−46] The percentage of calcite crystals in different orientations (*hkl*) was estimated according to the following equation:

$$\%\ hkl = \frac{I_{hkl}/I^*_{hkl}}{\sum_{hkl}(I_{hkl}/I^*_{hkl})} \times 100 \qquad (1)$$

The calculation results are listed in Table 1. It was found that different precipitation systems resulted in different orientational uniformity of calcite crystals. In the aqueous solutions of 1.0 g/L PVP, the predominant nucleating planes of calcite are (116), (024), (018), (122), (104); in 5.0×10^{-3} M SDS solutions they are (024), (113), (116), (104), (110); whereas in the 1.0 g/L PVP + 5.0×10^{-3} M SDS systems they are (024), (110), (116), (104), (018). These indicate the synergistic effect of polymer and surfactant in crystallization media.

3.4. Influence of PVP concentration on $CaCO_3$: Generally, the effect of organics on the crystallization habit of $CaCO_3$ should be related to the affinity between organic molecules and calcium ions.[47] Although it has been reported in our previous works that the presence of uncharged PVP increases the transformation rate from spherical vaterite to rhombohedral calcite,[22] it is difficult to correlate their activity in crystallization to polymer structure since they mostly occur in random-coil conformations. For example, the presence of 1.0 g/L PVP resulted in the major polydispersed calcite and the minor spherical vaterite, which resembles those precipitated from "pure water" (data not shown). Moreover, the organic templates must be shape-persistent under crystal growth conditions to be invariant during the nucleation stage.[48]

Upon these considerations, SDS concentration was fixed at 5.0×10^{-3} M to discuss the influence of PVP concentration on the crystallization and aggregation of $CaCO_3$. At higher PVP concentrations than 1.0 g/L, the plot of γ against log[SDS] showed lower CAC values, for example, the CAC value in the presence of 100 g/L PVP is ca. 5.5×10^{-4} M. Although SDS micelles could coexist in these crystallization systems,[1] it is obvious that surface tension results indicate the formation of PVP/SDS supramolecules.

Figure 4A showed that the $CaCO_3$ crystalline aggregates precipitated from the aqueous solution of 5.0×10^{-3} M SDS exhibited spherical morphology. The average size of these hollow spheres sampled in the presence of 100.0 g/L PVP (6.5 ± 0.8 μm in diameter, Figure 4B) is bigger than that in the absence of 100.0 g/L PVP (4.4 ± 0.8 μm in diameter, Figure 4A). This implies that different spherical templates functionalize in the crystallization systems. The insert in Figure 4B shows a TEM image of a nanosized particle around these spheres. The electron diffraction pattern corresponds to the [001] plane of rhombohedral crystals perpendicular to the zone axis, indicating that these aggregates are comprised of calcite particles.

It is interesting that the hollow spherical calcite resulting from the pure SDS micellar system (Figure 5A) has a thinner and more refined shell than that precipitated from the system of PVP/SDS supramolecules (Figure 5B). It might be due to the former organic precursor (SDS micelle) possessing more active sites of sulfate groups on its spherical surface than the bead of PVP/SDS supramolecules.[49] Another reason is that the presence

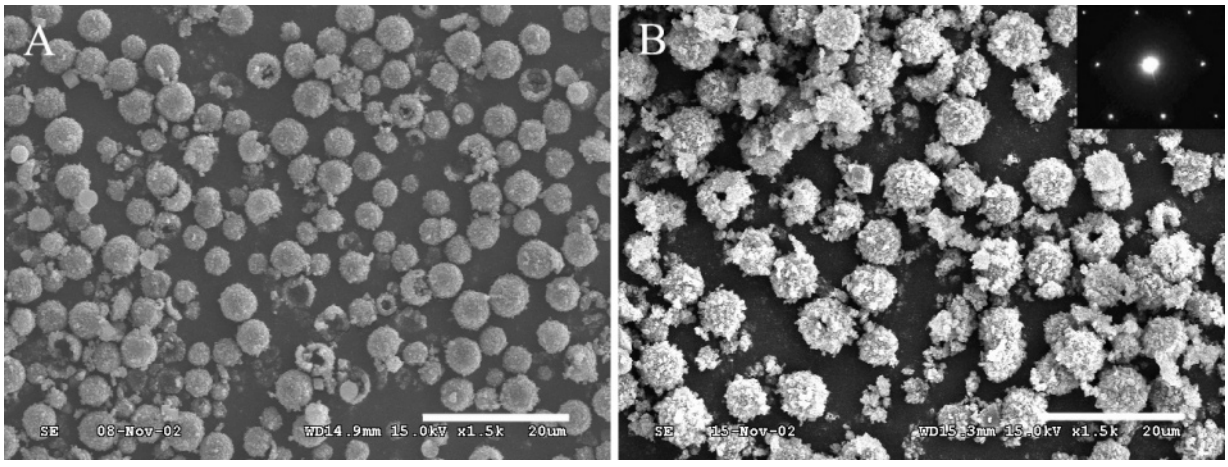

Figure 4. SEM images of $CaCO_3$ crystals precipitated from the SDS micellar system (A) and the aqueous solution of 5.0×10^{-3} M SDS + 100.0 g/L PVP (B), respectively. The insert is the electron diffraction patterns of a small particle of rhombohedral calcite showing the TEM image plane perpendicular to the [001] zone axis. Bar = 20 μm.

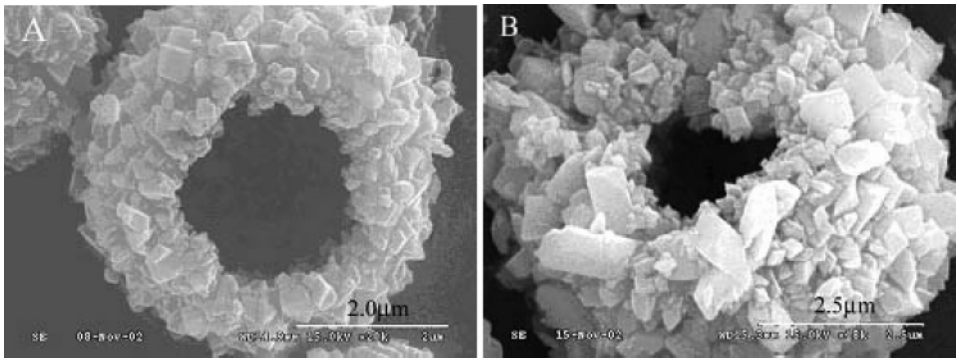

Figure 5. SEM images of $CaCO_3$ hollow spheres obtained from SDS micellar systems in the absence (A) and presence (B) of PVP, respectively.

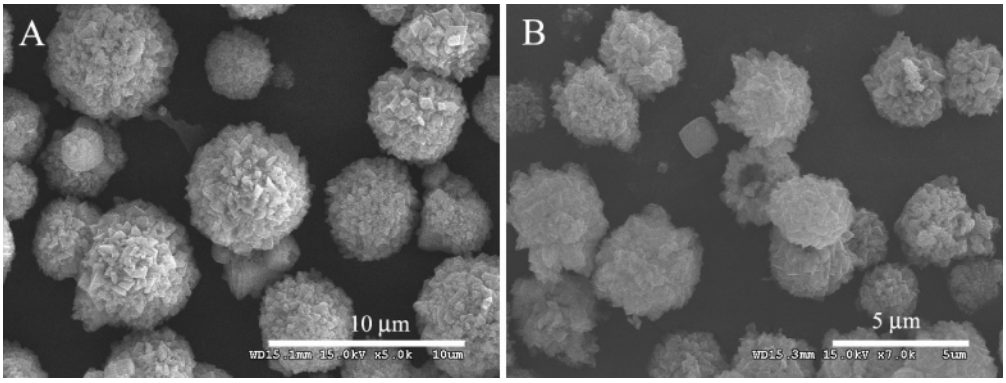

Figure 6. SEM images of $CaCO_3$ crystals sampled from 5.0×10^{-3} M SDS solutions in the absence (A) and presence (B) of 50.0 g/L PVP. It should be emphasized that, during the 10-h crystallization process, these incubation systems were kept still after 1 min mixing of reactants.

of PVP molecules causes the nucleation density and dispersion capability of $CaCO_3$ particles to increase.[22]

It should be pointed out that the values of the inner diameter of the hollow spherical calcite (ca. 1.0 μm) are incompatible with those of the maximum external diameters of organic precursors (ca. 1.8 nm).[50] It is speculated that the inner diameters of hollow spherical calcite matched the size of the initially formed amorphous intermediates outside of the organic precursors. And then, following dissolution of the amorphous $CaCO_3$ solids, the sequent crystallization, growth, and aggregation processes resulted in the big inner space.

3.5. Mechanism: From the above discussion, the structural relationship between organic self-assemblies and the growing minerals is still not so convincing. Another speculation is that the air bubbles generated by stirring serve as micron-sized templates. As a surface-active agent, SDS molecules prefer to distribute at the air/liquid interface. The air bubble stabilized by SDS molecules or PVP−SDS mixtures might also lead to the formation of these $CaCO_3$ superstructures.

After rapidly mixing $CaCl_2$ and Na_2CO_3 solutions, the crystallization system was kept still for 10 h. Then, the obtained $CaCO_3$ crystals were characterized for comparative purposes (Figure 6). In the absence (Figure 6A) or presence (Figure 6B) of PVP, the formation of hollow spherical aggregates demonstrates the effectiveness of spherical templates in the $CaCO_3$ crystallization process. Notably, no effect of bubble-template on the resulting crystals was observed. The average size of these hollow spherical aggregates obtained in the absence of 50.0 g/L PVP is 4.6 ± 1.2 μm in diameter, while that in the presence of 50.0 g/L PVP is 3.1 ± 0.6 μm. The polydisperse degree of particle size for former spheres (from 1.6 to 7.3 μm) is bigger than that for the later (from 1.8 to 4.8 μm), which proves the PVP dispersion capability for the solid particles.

It should also be noticed that: the stirring has almost no influence on the average size of the core−shell structures obtained from "pure" SDS micellar systems (Figures 4A and 6A), but has a relatively larger effect on the particle size of $CaCO_3$ obtained from the aqueous solution of the PVP and SDS mixture (Figures 4B and 6B). This might be due to the stirring exerting less effectiveness on SDS micellar templates than on the PVP/SDS supramolecular configurations. Actually, this could be easily proved by a rheological method.

4. Conclusions

In these spontaneous precipitation systems of $CaCO_3$, PVP molecules associate with SDS molecules to form different self-organized structures at different SDS concentrations. The surface density of functional groups of organic precursors plays an important role in the morphological control of calcite aggregates. Of course, the role of the uncharged polymer is also significant, because only in the presence of SDS can the flower-shaped calcite aggregates not be obtained.

In summary, the presented results partly illuminate that the grown $CaCO_3$ aggregates copy the symmetry and dimensionalities of organic precursors.[51] Nevertheless, the crystallization and aggregation mechanism, such as the enrichment of calcium ions on polymer/surfactant superstructures, is still unclear. However, it opens a new avenue for the synthesis of highly functional materials applying the biomimetic mineralization approach.

Acknowledgment. Financial support from the Natural Science Found of Shandong Province (Y2004B05), the Excellent Young Scientist Awarding Fund of Shandong Province (02BS115), and the National Natural Science Foundation of China (20471064) is gratefully acknowledged.

References and Notes

(1) Leontidis, E.; Kyprianidou-Leodidou, T.; Caseri, W.; Robyr, P.; Krumeich, F.; Kyriacou, K. C. *J. Phys. Chem. B* **2001**, *105*, 4133−4144.

(2) Currey, J. D.; Talor, J. D. *J. Zool.* **1974**, *173*, 395−406.
(3) Currey, J. D.; Kohn, A. J. *J. Mater. Sci.* **1976**, *11*, 1615−1623.
(4) (a) Currey, J. D. *J. Zool.* **1976**, *180*, 445−453. (b) Currey, J. D. *Proc. R. Soc. London B* **1977**, *196*, 443−463. (c) Currey, J. D. *J. Zool.* **1979**, *188*, 301−308. (d) *The Mechanical Properties of Biological Materials*; Vincent, J. F. V., Currey, J. D., Eds.; Cambridge University Press: Cambridge, UK, 1980; pp 75−97.
(5) Watabe, N. In *Progress in Crystal Growth and Characterization of Materials*; Pamplin, B. R., Eds.; Pergamon Press: New York, 1981; Vol. 4, pp 99−147 and references therein.
(6) Elfil, H.; Roques, H. *Desalination* **2001**, *137*, 177−186.
(7) Cechova, M.; Alinc, E. B.; van de Ven, T. G. M. *Colloids Surf., A* **1998**, *141*, 153−160.
(8) Tsuno, H.; Kagi, H.; Akagi, T. *Bull. Chem. Soc. Jpn.* **2001**, *74*, 479−486.
(9) Walsh, D.; Mann, S. *Nature* **1995**, *377*, 320−323.
(10) Fendler, J. H.; Meldrum, F. C. *Adv. Mater.* **1995**, *7* (7), 607−632.
(11) Marentette, J. M.; Norwig, J.; Stöckelmann, E.; Meyer, W. H.; Wegner, G. *Adv. Mater.* **1997**, *9* (8), 647−651.
(12) Küther, J.; Tremel, W. *Thin Solid Films* **1998**, *327−329*, 554−558.
(13) Küther, J.; Seshadri, R.; Knol, W.; Tremel, W. *J. Mater. Chem.* **1998**, *8* (3), 641−650.
(14) Küther, J.; Nelles, G.; Seshadri, R.; Schaub, M.; Butt, H.-J.; Tremel, W. *Chem. Eur. J.* **1998**, *4* (9), 1834−1842.
(15) Vučak, M.; Perić, J.; Pons, M. N.; Chanel, S. *Powder Technol.* **1999**, *101*, 1−6.
(16) Falini, G. *Int. J. Inorg. Mater.* **2000**, *2*, 455−461.
(17) Cölfen, H.; Antonietti, M. *Langmuir* **1998**, *14*, 582−589.
(18) Cölfen, H.; Qi, L. *Chem. Eur. J.* **2001**, *7*, 106−116.
(19) Malkaj, P.; Chrissanthopoulos, A.; Dalas, E. *J. Cryst. Growth* **2002**, *242*, 233−238.
(20) Donners, J. J. J. M.; Heywood, B. R.; Meijer, E. W.; Nolte, R. J. M.; Sommerdijk, N. A. J. M. *Chem. Eur. J.* **2002**, *8* (11), 2561−2567.
(21) Zheng, M.; Gu, M.; Jin, Y.; Wang, H.; Zu, P.; Tao, P.; He, J. *Mater. Sci. Eng. B* **2001**, *87*, 197−201.
(22) Wei, H.; Shen, Q.; Zhao, Y.; Wang, D.-J.; Xu, D.-F. *J. Cryst. Growth* **2003**, *250*, 516−524.
(23) Bujan, M.; Sikirić, M.; Filipović, N.; Vdović, N.; Garti, N.; Füredi-Milhofer, H. *Langmuir* **2001**, *17*, 6461−6470.
(24) Škrtić, D.; Filipović-Vinceković, N. *J Cryst. Growth* **1988**, *88*, 313−320.
(25) Škrtić, D.; Filipović-Vinceković, N.; Babić-Ivančić, V.; Tušek-Božić, Lj. *J Cryst. Growth* **1993**, *133*, 189−195.
(26) Tunik, L.; Addadi, L.; Garti, N.; Füredi-Milhofer, H. *J. Cryst. Growth* **1996**, *167*, 748−755.
(27) Antonelli, D. M. *Microporous Mesoporous Mater.* **1999**, *28*, 505−510.
(28) Zheng, X.; Xie, Y.; Zhu, L.; Jiang, X.; Yan, A. *Ultrason. Sonochem.* **2002**, *9*, 311−316.
(29) Braun, P. V.; Stupp, S. I. *Mater. Res. Bull.* **1999**, *34*, 463−469.
(30) Kandori, K.; Kon-no, K.; Kitahara, A.; Fujiwara, M.; Tamura, T. In *Surfactants in Solution*; Mittal, K. L., Ed.; Plenum: New York, 1989; Vol. 10, p 253.
(31) Arai, H.; Murata, M.; Shixoda, K. *J. Colloid Interface Sci.* **1971**, *37*, 223−227.
(32) Chari, K.; Hossain, T. Z. *J. Phys. Chem.* **1991**, *95*, 3302−3305
(33) Purcell, I. P.; Thomas, R. K.; Penfold, J.; Howe, A. M. *Colloids Surf., A* **1995**, *94*, 125−130.
(34) Eastman, J. R.; Goodwin, J. W.; Howe, A. M. *Colloids Surf., A* **2000**, *161*, 329−338.
(35) Hild, A.; Séquaris, J.-M.; Narres, H.-D.; Schwuger, M. *Colloids Surf., A* **1997**, *123−124*, 515−522.
(36) Shimayashi, S.; Uno, T.; Nakagaki, M. *Colloids Surf., A* **1997**, *123−124*, 283−295.
(37) Li, F.; Li, G.-Z.; Xu, G.-Y.; Wang, H.-Q.; Wang, M. *Colloid Polym. Sci.* **1998**, *276*, 1−10.
(38) Dutt, G. B.; Stam, J. V.; Schryver, F. C. *Langmuir* **1997**, *13*, 1957−1963.
(39) Liang, P.; Shen, Q.; Zhao, Y.; Zhou, Y.; Wei, H.; Lieberwirth, I.; Huang, Y. P.; Wang, D. J.; Xu, D. F. *Langmuir* **2004**, *20*, 10444−10448.
(40) Naka, K.; Chujo, Y. *Chem. Mater.* **2001**, *13*, 3245−3259.
(41) Falini, G.; Albeck, S.; Weiner, S.; Addadi, L. *Science* **1996**, *271*, 67−69.
(42) Dupont, L.; Portemer, F.; Figlarz, M. *J. Mater. Chem.* **1997**, *7* (5), 797−800.
(43) Levi, Y.; Albeck, S.; Brack, A.; Weiner, S.; Addadi, L. *Chem. Eur. J.* **1998**, *7* (3), 389−396.
(44) The standard XRD spectrum for randomly oriented calcite powder in the manipulation software of the Rigaku D/max-2400 powder X-ray diffractometer.
(45) Aizenberg, J.; Black, A. J.; Whitesides, G. M. *J. Am. Chem. Soc.* **1999**, *121* (18), 4500−4509.
(46) Damle, C.; Kumar, A.; Sainkar, S. R.; Bhagawat, M.; Sastry, M. *Langmuir* **2002**, *18*, 6075−6080.
(47) Hosoda, N.; Kato, T. *Chem. Mater.* **2001**, *13*, 688−693.
(48) Donners J. J. J. M.; Nolte R. J. M.; Sommerdijk N. A. J. M. *J. Am. Chem. Soc.* **2002**, *124*, 9700−9701.
(49) Xu, G. Y.; Yang, Y. L.; Zhang, L.; Yuan, S. L.; Li, G. Z. *Mater. Sci. Eng. C* **1999**, *10*, 47−50.
(50) Evans, D. F.; Wennerström, H. In *The Colloidal Domain Where Physics, Chemistry, Biology, and Technology Meet*; Evans, D. F., Wennerström, H., Eds.; VCH Publishers Inc.: New York, 1994; pp 1−35.
(51) Schüth, F. *Chem. Mater.* **2001**, *13*, 3184−3195.